DOI 10.1515/nanoph-2013-0055 — Nanophotonics 2014; 3(3): 181–201

Review article

Cheng-Wei Qiu*, Darwin Palima, Andrey Novitsky, Dongliang Gao, Weiqiang Ding, Sergei V. Zhukovsky and Jesper Gluckstad

Engineering light-matter interaction for emerging optical manipulation applications

Abstract: In this review, we explore recent trends in optical micromanipulation by engineering light-matter interaction and controlling the mechanical effects of optical fields. One central theme is exploring the rich phenomena beyond the now established precision measurements based on trapping micro beads with tightly focused beams. Novel synthesized beams, exploiting the linear and angular momentum of light, open new possibilities in optical trapping and micromanipulation. Similarly, novel structures are promising to enable new optical micromanipulation modalities. Moreover, an overview of the amazing features of the optics of tractor beams and backward-directed energy fluxes will be presented. Recently the so-called effect of negative propagation of the beams (existence of the backward energy fluxes) has been confirmed for X-waves and Airy beams. In the review, we will also discuss the negative pulling force of structured beams and negative energy fluxes in the vicinity of fibers. The effect is achieved due to the interaction of multipoles or, in another interpretation, the momentum conservation. Both backward-directed Poynting vector and backward optical forces are counter-intuitive and give an insight into new physics and technologies. Exploiting the degrees of freedom in synthesizing novel beams and designed microstructures offer attractive prospects for emerging optical manipulation applications.

Keywords: Optical force; synthesized beams; micromanipulation; optomechanical effects; tractor beam; force-sensing microstructure.

PACS: 87.80.Cc; 42.50.Wk; 42.25.Dd; 37.10.Pq

***Corresponding author: Cheng-Wei Qiu,** Department of Electrical and Computer Engineering, National University of Singapore, 4 Engineering Drive 3, Singapore 117583, e-mail: eleqc@nus.edu.sg; chengwei.qiu@gmail.com
Darwin Palima, Sergei V. Zhukovsky and Jesper Gluckstad: Department of Photonics Engineering, Technical University of Denmark, ØrstedsPlads, Building 343, 2800 Kgs. Lyngby, Denmark
Andrey Novitsky: Department of Theoretical Physics, Belarusian State University, Nezavisimosti Avenue 4, 220050 Minsk, Belarus
Dongliang Gao and Weiqiang Ding: Department of Electrical and Computer Engineering, National University of Singapore, 4 Engineering Drive 3, Singapore 117583

Edited by Dennis Couwenberg

1 Introduction

Mechanical effects are among the most important aspects of light-matter interaction. The mechanical effects of optical fields provide a novel way to transport and manipulate objects in a highly precise way, which was witnessed over the last two decades (e.g., see reviews [1–4]). The first observation of the mechanical effect of light on matter can be traced back to more than 400 years ago [5, 6], when J. Kepler saw the comet tails point away from the sun. More than 250 years later [7], J. C. Maxwell published his theory of classical electrodynamics, and people came to know that the momentum carried by light can be transferred to an object, pushing it forward, just like a comet tail. Momentum conservation is one of the basic concepts to understand the optical forces and optical trapping between light and objects. Since the invention of the laser in 1960, optical manipulation has developed intensively, and many significant applications [3] have become indispensable tools in scientific research and everyday life. A decade later, Ashkin [8] used focused laser beams to accelerate and trap microparticles. In 1986, Ashkin and his coworkers [9] first demonstrated optical trapping by gradient force from a strongly focused beam, known as *optical tweezers*. Since then, optical manipulation has been intensely developed in various structures and devices, such as optical fibers [10], waveguides [11], optical nanoapertures [12], and so on [13–15]. More recently, new trends and themes are emerging rapidly, which shine new light on optical manipulation both in theory and applications.

All optical forces originate from transfer of momentum when light interacts with matter. However, it is not uncommon to encounter different components of the optical force in literature. One such component is the scattering force [16]. The scattering force in the absence of intensity gradients and, in this case, its direction can be modified by applying a phase gradient [17] to tilt local wavevectors and create a transverse component of the scattering force. Another component is the gradient force that originates from the intensity gradient in free space [3, 9], in nanostructures [18, 19]. Optically induced mechanical effects can also result indirectly, e.g., in photophoresis [20], where nonuniform laser heating of particles, typically aerosols, results in asymmetric fluidic forces, which are much stronger than the direct optical force, and can manipulate the particles over relatively much larger distances. This kind of force, however, is beyond the scope of this current paper. On the other hand, all the components involved in the interaction of light with matter can be divided into three parts: one part is the incident beam, the second part is the manipulation of target object, and the third part is the background. Therefore, all the features of optical forces can be tailored by engineering those three parts, either individually or simultaneously. In this context, new trends and themes in optical manipulation are classified and reviewed in the current paper.

One trend in optical manipulation is the use of synthesized optical beams, rather than Gaussian beams only. Such synthesized beams include phase gradient beams [17], vortex beams [21, 22], non-diffracting beams [23], accelerating beams [24], self-healing beams [25], or more complex structured beams achieved by encoding holograms on spatial light modulators (SLM) [26, 27]. Among these synthesized beams, a phase-gradient force can be generated, which provides a complementary force to the intensity-gradient force. The synthesized beams enable a much greater freedom in object manipulation than the Gaussian beams.

Aside from the optical parameters, the geometric parameters (i.e., the shape of the object) also play an important role in the interaction of light and matter. Therefore, another new trend in the optical manipulation is to design objects with specified geometric shapes. For example, when the object is an ideal sphere, only a simple forward motion is expected in a light field of a plane wave. However, when the object is cut and acquires asymmetry, it may move along other directions, e.g., a stable light lift [16]. Furthermore, when the object is more complex and carefully designed [28–30], it may act as an optical motor when illuminated by a light beam. Thus, the engineering of microstructure geometries provide further new ways for optical manipulation.

One may expect that when an object is illuminated by a beam having minimal gradient along its propagation (referred to as a "gradientless beam" subsequently), it will only be subjected to a "pushing" force directed along the beam, since the momentum of photons will be transferred to the object in the interaction process. Recently, however, a sharply counter-intuitive phenomenon has been found, i.e., a gradientless beam may *pull* the object "backwards" to the beam source [26, 31, 32], rather than push it away. The beams with this negative scattering force have been named "optical tractor beams", and are also found in the acoustic domain [33]. Considering the momentum conservation of the system, a negative or pulling force is obviously present only when the forward momentum of the incident beam is amplified. Still, both theoretical achievements and experimental realizations of tractor beams are extremely challenging. Up to now, only several methods have been proposed, which can be methodologically grouped into two general kinds. One method is to engineer the optical beams. Engineered beams include non-paraxial Bessel beams [34, 35] and superpositions ofplane waves or Bessel beams [36–38]. The other method is to use some special kind of materials, such as gain materials [39, 40], negative refractive index materials [41], optomagnetic materials [42]. Optical tractor beams provide a new route for long-distance optical manipulation using the negative scattering force.

In this paper, we briefly review the recent progress and novel trends in the field of optical manipulation. As mentioned above, we are not including the vast progress related to the optical tweezers, since it has been reviewed by many other authors elsewhere [2]. In Section 2, we briefly outline the basic theory and methods used in optical manipulation analysis, including the Poynting vector and Maxwell's stress tensor, which are tightly related to the optical forces. In Section 3, optical manipulation using synthesized beams is discussed, including phase-gradient, accelerating, and self-healing beams. In Section 4, we present the optical manipulation of micro-objects with designed geometries, which act as microtools, couplers of optical radiation to subwavelength components, or other functional elements. In the final two sections, we focus on a new topic in the optical manipulation, i.e., negative or pulling optical forces. In Section 5, we focus on the effects of the negative Poynting vector; in Section 6, we focus on the optical tractor beam, including its basic principles and several experimental configurations.

2 Particle micromanipulation

2.1 Mechanical micromanipulation with optical fields

The basic principle of optical micromanipulation can be described by the momentum conservation principle: When light changes its momentum upon interaction with matter, the rate of change of the optical momentum corresponds to an optical force exerted on the material. For example, it is relatively easy to qualitatively infer the direction of the optical force on a microsphere by observing the light deflection, e.g., in the simulated propagation of a focused field upon interacting with a microsphere, as shown in Figure 1A. Therefore, besides its conventional use as particle position indicator [45], the experimental measurements of the light deflections can also be used as indicators of momentum change, i.e., for direct measurement of the optical force [43, 46].

Despite this intuitively simple picture, analytical solutions of the optical force problem are, nonetheless, not available for arbitrary illumination and particle geometries, although these can be addressed by numerical models [47–50]. For instance, finite-difference time-domain (FDTD) simulations can solve Maxwell's equations to map out the electromagnetic field and calculate the force arising from the light-matter interaction. Moreover, useful insight can be derived using solutions of simple model systems such as homogeneous dielectric spheres in the Rayleigh (size$<<\lambda$) [51, 52], or ray optics (size$>>\lambda$) [53] regimes.

For an electromagnetic wave in free space characterized by electric field $\boldsymbol{E}$ and magnetic field $\boldsymbol{B}$, the Poynting vector, $\boldsymbol{S}=\boldsymbol{E}\times\boldsymbol{B}$, is typically associated with electromagnetic energy but it also plays a key role in describing the optical force (J. H. Poynting himself contributed scientifically to the description of optical force [54]). An electromagnetic wave has an associated linear momentum density, $\vec{m}$, which is related to the Poynting vector as,

$$\mathbf{m}=\frac{\boldsymbol{S}}{c^2}=\frac{1}{c^2}(\boldsymbol{E}\times\boldsymbol{B}), \tag{2.1}$$

Thus, one can visualize how the optical momentum evolves when focused light interacts with a dielectric microsphere (e.g., the transverse and axial components of the Poynting vector simulated in [44] are shown in Figure 1B and C, respectively). When an electromagnetic wave interacts with a small polarizable dielectric particle with dipole moment density $\boldsymbol{P}$, the Lorentz force density may be written as

$$\boldsymbol{f}=(\boldsymbol{P}\cdot\nabla)\boldsymbol{E}+\frac{\partial\boldsymbol{P}}{\partial t}\times\boldsymbol{B} \tag{2.2}$$

Some authors identify the first term with the (field) gradient force and the second term with the scattering force [55]. However, an alternative nomenclature can be derived if the terms are expanded and regrouped to yield, after time averaging [52],

$$\mathbf{f}=\frac{\alpha n_m}{2c}\nabla\mathrm{I}+\alpha n_m\frac{\Delta\boldsymbol{m}}{\Delta t} \tag{2.3}$$

where the first term now directly shows the force due to the intensity gradient. The second term now includes contributions from both terms in Eq. (2.2) to describe the rate of change of the linear momentum density, which is intuitively easier to associate with scattering.

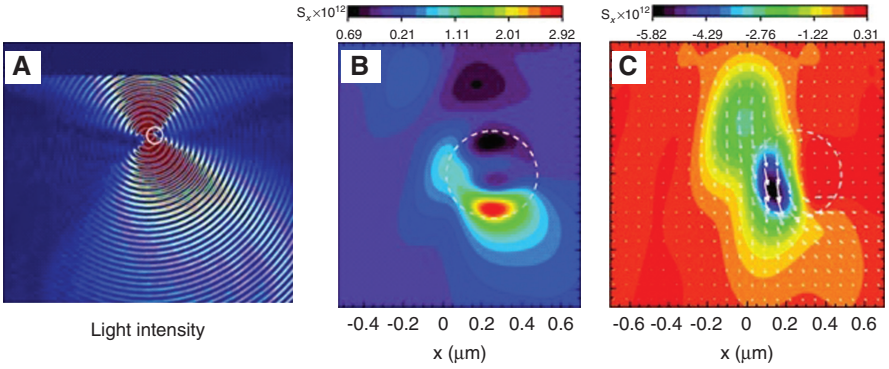

Figure 1 Linear optical momentum and optical force when light is focused off the center of a bead. (A) Simulated axial section showing the x-component of the electric field for a 1064 nm beam focused onto a 1-μm polystyrene sphere in water by a 1.3NA lens. The optical force can be deduced from the deflection of light due to the dielectric bead, which is indicative of the momentum change (adapted from [43]); (B) x-component of the Poynting vector, S_x; (C) z-component of the Poynting vector, S_z, with the vector field indicating the full Poynting vector (the simulations of this smaller microsphere are adapted from [44]).

Separating the optical force into these components provides a useful framework for understanding optical micromanipulation phenomena. Although the optical force is usually described as radiation pressure that pushes particles along the propagation direction of light due to scattering [8], the gradient force provides a way for light to pull particles towards the light source, which forms the basis for creating stable three-dimensional optical trapping sites [9]. Moreover, so-called tractor beam geometries – illumination and particle geometries that can result in pulling the particles towards the light source even without the gradient force – can be achieved when light is preferentially scattered forward, as will be discussed further in Sections 5 and 6, where we also consider magnetodielectric particles.

Instead of rewriting the force density in terms of gradient and scattering force components, we may instead write it in terms of the Maxwell stress tensor, $\tilde{T}$:

$$\boldsymbol{f}=\nabla\cdot\tilde{\boldsymbol{T}}-\frac{1}{c^2}\frac{\partial \boldsymbol{S}}{\partial t} \tag{2.4}$$

With the second term associated with the rate of change of the electromagnetic momentum density, the first term, the divergence of the Maxwell stress tensor, can be identified as a momentum flux. In numerical simulations where the total field (i.e., including the incident and scattered radiation) is considered, the second term vanishes with time-averaging and the optical force is obtained by the volume integral of the first term.

2.2 Experimental geometries and strategies

Experimental strategies can tailor the experimental geometry based on the available degrees of freedom in the illumination, particle and its environment to achieve the optical force required for targeting specific applications of optical micromanipulation. Tightly focused beams can create sharp intensity gradients to have stable trapping points for single beam optical tweezers [9]. Stable traps can also be created with dual beam traps that use counter propagating beams to create stable trapping points [3, 8, 56]. Beam modulation techniques are also available to generate dynamic beams for creating a reconfigurable trap or even multiple traps for moving particles along user-defined trajectories. Alternately, defined trajectories can also be generated using static beams, for instance in passive optical sorting that separate particles according to their optical properties [57–59].

Although the interplay between illumination, particle and environment provides a useful theoretical context for describing optical micromanipulation, actual experimental geometries can involve many different blocks or modules, as illustrated in Figure 2. We note that not all systems exploit the available degrees of freedom and, hence, not all components may be present in every optical micromanipulation system. However, this system's description provides a framework for making sense of the numerous activities within optical micromanipulation, which are viewed as attempts to optimize the different components. For example, one can target different modules in order to extend the achievable dynamic range of the optical forces. Examples are numerous. When targeting the modulation and delivery modules, correctly under filling microscope objectives with laser illumination can be used to optimize the available power [60]. Reaching the nanonewton (nN) optical force domain can either be done in the particle module using antireflection-coated beads [61], or in the source module by just using regular beads but replacing the light source with a short-pulsed laser [62]. Moreover, by moving beyond the standard microspheres, microfabrication-tailored particle shapes can be used to create optically steered microtools [63], which we will discuss further in Section 4. Tailored particle shapes can also achieve user-designed light deflection to engineer the optical force, e.g., partial refraction for achieving

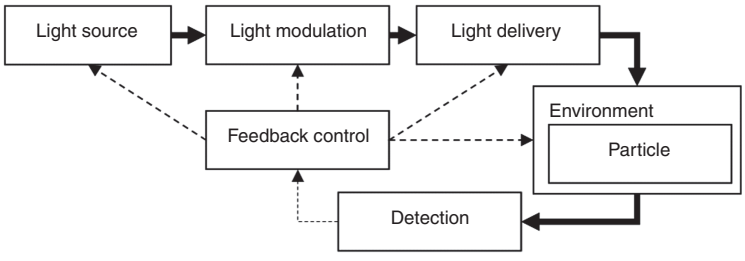

Figure 2 Experimental strategies can target certain applications by optimizing the available degrees of freedom in the different components of a generic optical micromanipulation system.

a stable optical lift [16] or even total internal reflection in waveguides for generating tailored optical forces [64, 65]. Optimizing the particle appears as a more recent trend compared to the earlier thrust in beam shaping and light modulation (see e.g., [66] for a review).

There are techniques that address several modules simultaneously. Designed fibers can both modulate and deliver light [67]. Light modulation can be targeted in order to correct for aberrations in the light delivery [68] and the trapping environment [69]. The trapping environment can also be designed and tweaked to aid in optical micromanipulation. Fluidic drag from microflows directed opposite to the optical force can separate particles according to their optical properties [70]. A hollow core waveguide can be even more universal: it can confine both the particle and optical radiation to achieve higher energy and momentum densities [71], also representing an innovation in light delivery. In principle, the feedback control module involves working with the different components simultaneously (e.g., particle position detection is used in feedback-based control of light modulation to improve optical manipulation [72]).

Having established the context of experimental optimizations based on the different generic components, we will now focus on the trends in using novel beams for illumination (Section 3) and the manipulation of designed microstructures (Section 4).

3 Micromanipulation with synthesized novel beams

The nature of light scattering off a given particle depends on the intrinsic properties of light such as energy (wavelength, amplitude) and momentum (polarization and wave vector), as well as extrinsic properties governing the spatial distribution of these quantities (where the intensity gradient also arises). Modulation and control over these properties provide a way to direct the course of optical micromanipulation. Static spatial light modulation can be achieved with lenses, axicons and other fixed optical elements while electrooptic modulators (i.e., Spatial light modulators) can address dynamic and reconfigurable spatial modulation to synthesize novel beams e.g., using computer-generated diffractive elements or generalized phase contrast [73, 74]. Synthesized beams can be tweaked to adjust the interplay between the gradient and scattering optical components to produce a wide range of optical micromanipulation possibilities.

3.1 Phase gradient and angular momentum

Apart from an extrinsic orbital angular momentum (the moment of linear momentum about an arbitrarily chosen axis), light can also have both an intrinsic orbital angular momentum (e.g., an optical vortex) and spin angular momentum (circular polarization) [75]. When light illuminates particles, it can exchange angular momentum with them to influence the dynamics of its rotational or orbital motion. In fact, Poynting's original proposals for verifying optical momentum and radiation pressure were based on angular momentum and rotation, rather than on linear momentum.

An optical vortex beam carries an intrinsic orbital angular momentum and is also referred to as a "doughnut beam" since its transverse profile appears as a bright ring surrounding a dark core. A particle can orbit the dark core of an optical vortex if it is small enough to get trapped by gradient forces along its bright ring. Once trapped, the transverse component of the local wave vector leads to a tangential/azimuthal component of the scattering force, which in turn leads to orbital motion along the trapping bright ring, as shown in Figure 3A [22]. Using a similar principle, beams can be synthesized in such a way that gradient forces constrain particles along light tracks where the scattering force from skewed wave vectors can simultaneously act to drive particles along these tracks. This type of optical micromanipulation can be said to arise due to optical forces from phase gradients [17] since, in this case, the transverse component of the wave vector is simply the transverse gradient of the phase. This transverse force from the phase gradient may be demonstrated by differently shaped beams that contain optical vortices [21, 27]. For example, a vortex-carrying beam reshaped to contain a triangular dark core in [27] is illustrated in Figure 3B. The optical force from phase gradients is, however, not restricted to optical-vortex-carrying beams but, in principle, should apply to beam produced by suitable beam shaping techniques that can independently control amplitude and phase distributions. Hence, based on this principle, a line pattern having a parabolic phase gradient can push two particles in opposite direction along the line trap, as shown in Figure 3C. This principle has also been demonstrated for three-dimensionally shaped light distributions such as knotted optical traps [76].

With optical forces arising from phase gradients, it is crucial to also have sharp axial gradients if optical axial confinement is required and it is undesirable to resort to other forces for axial confinement (e.g., gravity force or normal force from sample chamber). On the other hand, beams that completely lack axial gradients are

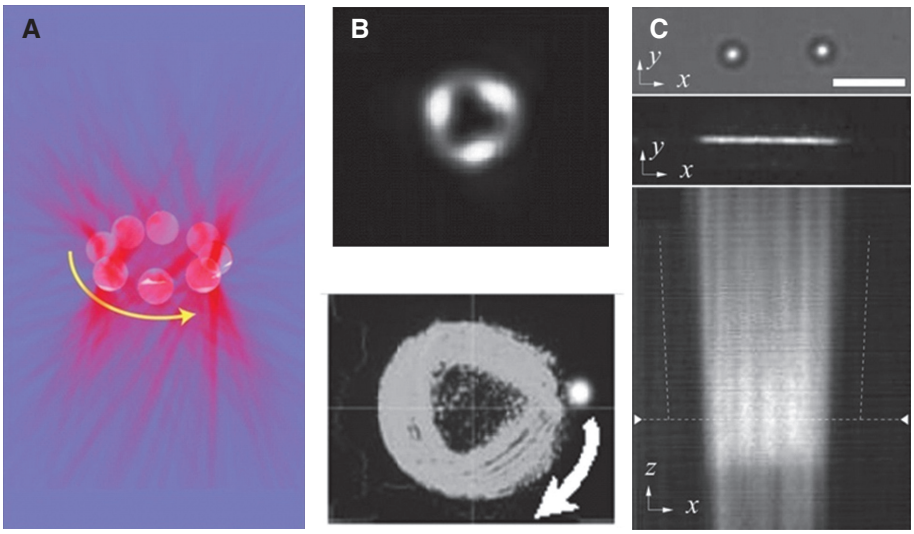

Figure 3 Motion of particles along light tracks due to skewed scattering and gradient forces. (A) A particle confined by gradient forces in the bright ring of an optical vortex can orbit that ring due to the azimuthal component of the scattering force (adapted from [22]); (B) similar principle for a triangular dark core of an optical vortex; (C) two microspheres (top) held by a line trap (middle) can be pushed along opposite directions when the line trap contains a parabolic phase gradient (manifests as a divergence in beam propagation shown in the bottom figure).

propagation invariant beams and can be of interest in other applications.

3.2 Propagation-invariant and self-healing beams

The transverse profiles of light beams typically evolve during propagation due to diffraction. However, some beams can maintain their transverse profile during propagation [77]. These propagation-invariant beams are interesting for a number of reasons. Certain parts of such beams, such as the central lobe of a Bessel beam, can seemingly have a diffraction-free character [23]: the light that diffracts out of the central lobe is replenished by diffraction from the other parts of the beam. This constant replenishment by diffraction from the other parts of the beam during propagation also leads to the seemingly self-healing or self-reconstructing behavior. For instance, the central spot in a zero-order Bessel beam self-replenishes after encountering obstructions during propagation (however, this replenishment can be hampered by blocking the outer rings of the Bessel beam, rather than its central spot, which would cause the central spot to lose its interesting properties). The absence of axial intensity gradients in propagation-invariant beams is also a useful property for isolating scattering-based axial optical forces.

Although the Bessel beam is a popular example of a propagation-invariant beam, various patterns can exhibit propagation invariance, even speckle-like patterns [78, 79]. The defining property is that the pattern is formed by a set of plane waves whose wave vectors lie on a cone, which corresponds to a spatial power spectrum that forms a ring (see Figure 4A). An intuitively simple experimental demonstration is based on an optical Fourier transform geometry where a light ring is placed at the front focal plane (the Fourier plane) of a lens [82]. Extending this Fourier optics approach, iterative algorithms can exploit the phase freedom in the Fourier ring to create different propagation-invariant patterns using Fourier holograms [80]. An example of such iteratively designed pattern is shown in Figure 5B. Instead of iteratively tailoring the phase of the plane wave, a random phase can be assigned to the phase waves in the light cone. Then, a nondiffracting speckle pattern is produced (e.g., see Figure 4C from [79]). In contrast, a Bessel beam of m^{th}-order is formed when the plane wave phases are designed to vary linearly around the wave-vector cone and the phase increments by $2\pi m$ after every turn (higher-order Bessel beam in Figure 4D is from [81]).

Propagation-invariant beams can be useful, e.g., for optical switching in active optical sorting experiments for selectively propelling a chosen particle away from a transverse laminar flow, where the beam can push the particle over a relatively longer range. In this case, the self-healing behavior can be useful when propelling a series of particles along the same path defined by light. However, the beams are typically invariant and self-healing only over

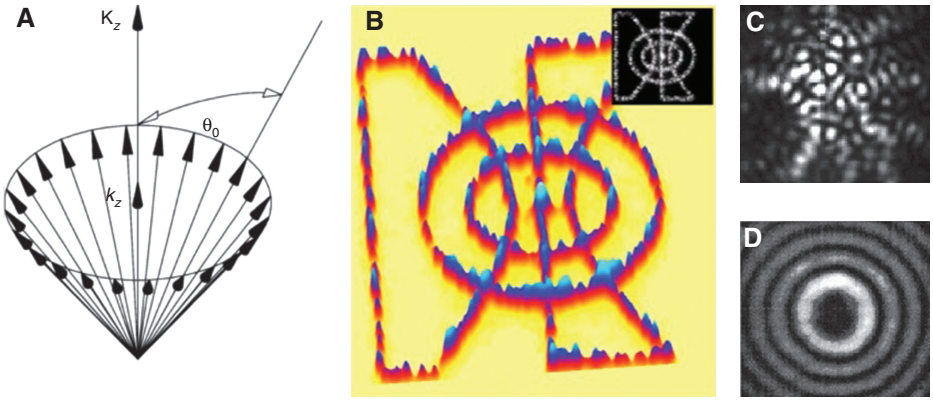

Figure 4 Nondiffracting beams (NDBs): (A) the angular spectrum showing a conical superposition of plane waves that creates NDBs; (B) iterative design that tweak the phases of the plane wave can create NDBs with arbitrary patterns (from [80]); (C) a nondiffracting speckle is formed when the plane waves have random phases (from [79]); (D) a Bessel beam of m^{th}-order is formed when the phase varies linearly around the cone and changes by $2\pi m$ times every turn (a 4^{th}-order Bessel beam is shown, from [81]). The radius of the inner ring increases with higher order and a 0-order Bessel beam has a bright center.

a limited range in experimental implementations because finite apertures truncate the infinite transverse extent (and energy) required by ideal propagation-invariant beams [85].

3.3 "Accelerating" beams

Just as diffraction can give the illusion of diffraction-free propagation of appropriately prepared beams, it can also create the illusion of accelerating beams: beams that can curve around corners, seemingly accelerating in free space and homogeneous media instead of propagating in a straight line. Examples of accelerating beam include Airy beams [24] and other parabolic beams [86], which are quasi-invariant beams: their intensity patterns appear invariant in an accelerating frame (i.e., the overall pattern is preserved but exhibits transverse shifts during propagation). The parabolic trajectory of an Airy beam in the axial section is shown in Figure 5A from [24], which also shows a finite quasi-invariant range due to truncations from limited apertures of the optical system.

Like the invariant beams in the previous section, the propagation of accelerating beams is completely governed by classical diffraction. The "self-healing" and "diffraction-free" properties of the main lobe are due to the diffraction from other parts of the beam. As shown in [87], the Poynting vectors in the other parts of the beam have transverse components (energy flow) pointing towards the central lobe. The quasi-invariance is robust to perturbations from scattering and turbulence but the central lobe exhibits regular diffraction broadening when all the other lobes are blocked. The transverse components of the Poynting vectors have corresponding momentum

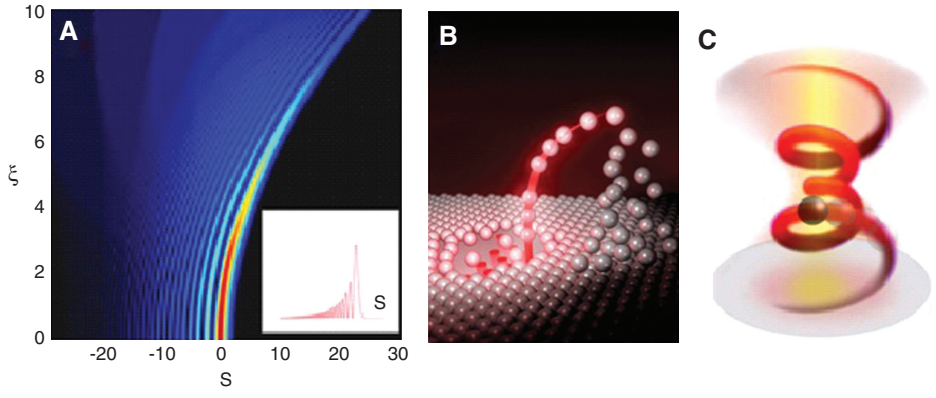

Figure 5 Accelerating beams (A) a finite-energy Airy beam is quasi invariant over a finite range [24]; (B) Airy beams can guide multiple particles along an accelerating trajectory [83]; (C) spiral beams, like the helico-conical beam can steer particles along a spiral trajectory [84].

flow (cf. force from phase gradients). Thus, when incident on an array of particles, the phase and intensity gradient from the minor lobes tend to bring particles towards the brightest spot, which can then propel them along the accelerating path [83]. The quasi-invariance again leads to self-healing properties of the Airy beam, which can be useful for guiding multiple particles along the curved path.

Other accelerating beams such as those produced by a superposition of higher-order Bessel beams having unequal orders also exhibit quasi invariance, but in a rotating coordinate system, hence resulting in a beam that propagates along a spiral path and have been called helicon beams [88, 89] and solenoid beams [26]. There are also diffracting accelerating beams, e.g., the helico-conical beam (HCB) – created e.g., using Fourier holograms having a transmission function of the form $\exp[il\theta(K\text{-}r/r_0)]$, which is characterized by a nonseparable helical (azimuthal) phase and the conical (radial) phase [90]. Despite their diffractive behavior, HCBs have also been shown to self-reconstruct after encountering an obstruction [25]. Helico-conical beams can work as "optical twisters" that can steer microparticles along spiral trajectories during optical micromanipulation [84].

4 Micromanipulation of designed microstructures

The previous section identified different techniques for optimizing optical forces by synthesizing improved beams. However, under any kind of illumination, the light scattering and the optical force would depend both on the material (material constants) and on the geometry (spatial distribution and geometric shape) of the illuminated particle. Homogeneous spherical beads are popular in optical micromanipulation studies both for the experimental predictability and theoretical tractability. However, together with conventional microfabrication technologies, the laser direct-write methods for three-dimensional fabrication (e.g., multiphoton polymerization [91]) open new possibilities for creating synthetic microstructures of various shapes for wide range of applications [92]. Hence, it is worth examining structure-based degrees of freedom for optimizing optical micromanipulation [93]. Besides potential improvements in systems for delivering and measuring optical forces, these optimizations can lead to as well as expand the range of modalities for exploiting optical forces. One of the core ideas is to use fabrication technologies for shaping microstructures that redirects optical momentum by design to achieve the desired mechanical effects from optical forces [64].

4.1 Microstructures optimized for force sensing and delivery

Force-calibrated optical tweezers systems are, to date, the main success story regarding the application of optical forces. Thus, it makes sense to explore particle-based optimizations when trapping small dielectric spheres, which are employed in these systems. Is there anything left to be optimized on the microbead? Indeed, a recent study shows that something as simple as optimizing the bead size (to match the trapping beam) can lead to improvements (reduced errors) when doing force measurements in optical traps [94]. Another conceptually simple (but technique-intensive) approach is to apply anti-reflection coating onto high-refractive-index microspheres to achieve stability and nanonewton optical forces [61]. These enhancements can be applied when trapping the typically spherical handles of more complex structures such as components in micro-assembly [95] or optically-steered microtools [96, 97]. However, more complex structures will require a different calibration than simple spheres due to difference in their dynamics [97].

Microfabrication is also advancing developments in optically driven micromotors [28–30, 98, 99]. Optical micromotors can, among others, drive fluids in micropumps [29], establish a velocity field for applying hydrodynamic shear [30], or, upon proper calibration, work as miniature instruments for probing fluid properties [99]. Interestingly, fluid-mediated optomechanics can be achieved not only by delivering optical momentum but also by optical energy, e.g., via pulsed laser-induced cavitation bubbles [100].

An ongoing goal is to use microfabrication to shape the object according to the demands of specific optical micromanipulation applications [93]. Besides optimizing microspheres, an alternative would be to exploit microfabrication to come up with new ways of creating optical manipulation handles. Veering away from analytically solvable spheres means an increasing role of numerical optimization in the design process. Some of these attempts are illustrated in Figure 6. Figure 6A illustrates that a plane wave can exert a stable transverse component using Fresnel reflection and refraction on a half-cylinder [16]; Figure 6B shows that a microstructure containing waveguides can be optically manipulated using the optical force arising from the light deflections caused by the waveguides [64]. Figure 6C shows that focused light

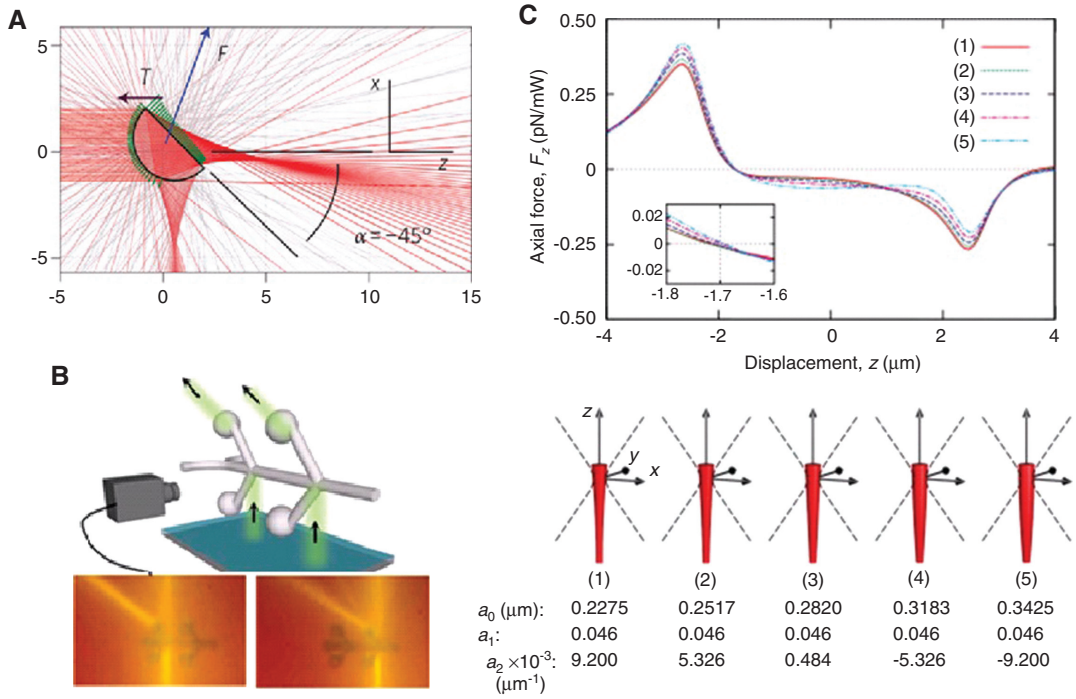

Figure 6 Exploring alternative microstructure geometries for exerting constant force; (A) gradient free (plane wave) illumination leading to stable optical lift; (B) a structure containing waveguides can be optically manipulated by exploiting the optical force arising from the light deflected by the waveguides; (C) Focused light can exert constant force on a tapered microrod.

can exert an optical pulling force on a tapered rod within a certain range of displacements [101].

4.2 Trapped microstructures for light delivery

One goal of nanophotonics technologies is to create functional tools that can perform tasks in the submicrometer domain. Here the classical diffraction barrier presents a challenge for techniques based on far-field optics. In STED microscopy [102], resolution enhancement is mediated by a second light source that shuts off fluorescence around a nanometric core where fluorescence is then localized using only far-field optics. In optical micromanipulation, a way to jump the diffraction hurdle is using structure-mediated micro-to-nano coupling [92]. Here, a trapped microstructure, big enough to be amenable to optical trapping, serves to tap onto a diffraction limited beam and channel its effects onto subwavelength regime. One example is to optically manipulate a relatively large microstructure to direct its subwavelength tip for SPM-like imaging [96].

The structure-mediated approach also makes it possible to tap into diffraction limited light to deliver it to subwavelength targets, as shown by the approaches illustrated in Figure 7. In Figure 7A, a microbead trapped by an infraredbeam serves as a microlens for focusing an ultraviolet laser beam to enable subwavelength direct-write material nanopatterning [103]. Using a two-photon polymerized microstructure having optical trapping handles and an embedded waveguide, a second laser beam can be guided onto its tip to selectively excite fluorescence on a microsphere situated within a vertical stack [63]. The waveguide is bidirectional and can also redirect light captured by its tip. Optical traps can also manipulate nanowires, albeit with limited orientational control since the nanowires tend to align along the optical axis. Figure 7C shows that by resting one tip of a nanowire on a fluorescent bead, trapping the other tip can, with the proper choice of the nanowire material, generate second harmonic light, which can be guided along the nanowire to excite fluorescence on the bead [104].

5 Negative Poynting vector: force becoming negative?

5.1 Fundamentals of reversed Poynting vector

The Poynting vector is commonly associated with the flow of the energy of a wave. In the simplest case the

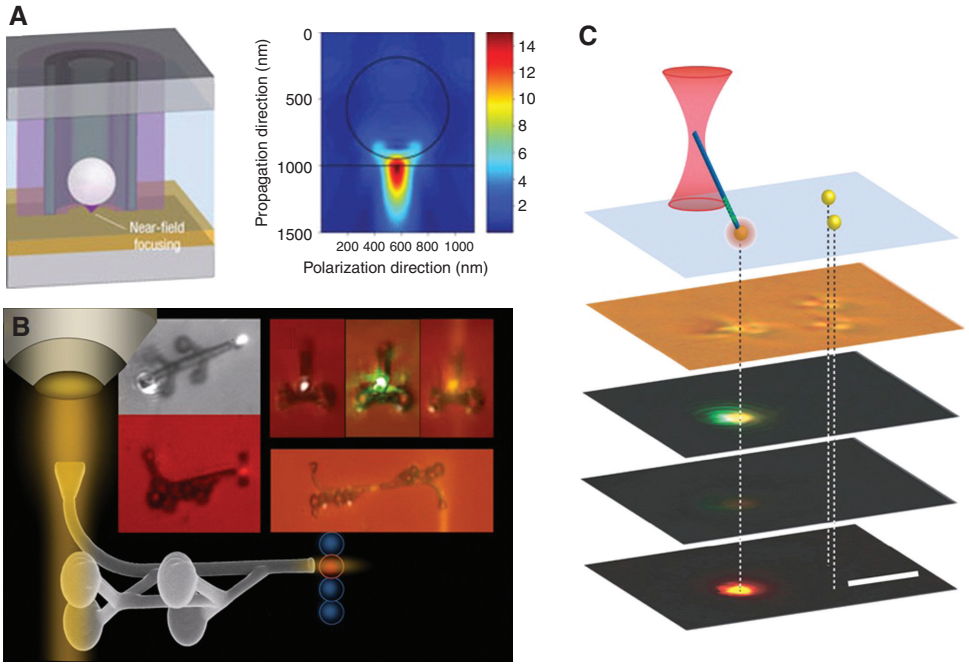

Figure 7 Trapped microstructures for light delivery. (A) An infrared-beam-trapped microbead focuses an ultraviolet laser beam for sub-wavelength direct-write material nanopatterning [103]; (B) a trapped microstructure guides a second laser beam to selectively excite a microsphere within a vertical stack (left inset: top- and side-view experiment snapshots; right inset: tip emissions for different input wavelengths) [63]; (C) a nanowire, trapped on one tip, guides second-harmonic generated light to the other tip resting on a bead and excites fluorescence in it [104].

time-averaged Poynting vector of a plane wave $\boldsymbol{S}=\varepsilon_0 c|\boldsymbol{E}|^2\boldsymbol{k}/2$ is constant and positive in the sense that its direction coincides with that of the wavevector $\boldsymbol{k}$. However, in general, the laser radiation can be modeled and realized in more intricate ways. It is often a paraxial electromagnetic beam – superposition of plane waves with wavevector directions close to the optical axis z. The Poynting vector component of paraxial beams naturally oscillates in the vicinity of the constant value. The oscillation becomes stronger when the angles between the wavevectors and the z axis increase. Thus, for full-vectorial non-paraxial beams the local value of the Poynting vector component can take negative values, i.e., point in the opposite direction with respect to the beam propagation (see Figure 8A).

Negative Poynting vector component (energy flux density) does not mean that the overall beam energy flows in the direction opposite to the wavevector direction like in metamaterials with negative refraction. The total energy flux $\Phi=\int \boldsymbol{S}d\boldsymbol{s}$ remains positive, but the local value of $\mathbf{S}d\mathbf{s}$ can reverse sign. In other words, the energy fluxes computed over a selected part of the whole infinite plane z=const can take both positive and negative values, though they have no immediate physical meaning [105]. Nevertheless, if it were feasible to absorb all radiation except the selected area, one could think of producing a beam with reversed Poynting vector and reversed energy flux [106].

It would be perfect if the reversed Poynting vector could be detected using nanoparticles. Time-averaged optical force for the Rayleigh-regime spherical particles (with radius much less than the radiation wavelength) can be presented as the sum of the gradient force (due to the spatially distributed intensity) and the nonconservative force. The nonconservative force is the sum of the radiation pressure force F_{rp}, proportional to the Poynting vector at the point of particle position, and the gradient-phase force F_{gp} [32, 107]. For non-diffractive waves the intensity along the z axis is constant, so the gradient force vanishes. The radiation pressure optical force can be negative due to the negative Poynting vector component, but its effect is often blocked by F_{gp}. So, for the gradientless electromagnetic beams the optical force is negative if $F_{rp}+F_{gp}<0$.

In the following section, we will consider some typical examples of the systems where the Poynting vector becomes reversed. These are the superposition of two plane waves (Figure 8B), non-paraxial Bessel beams (Figure 8C), non-paraxial Airy beams (Figure 8D), and fiber modes (Figure 8E).

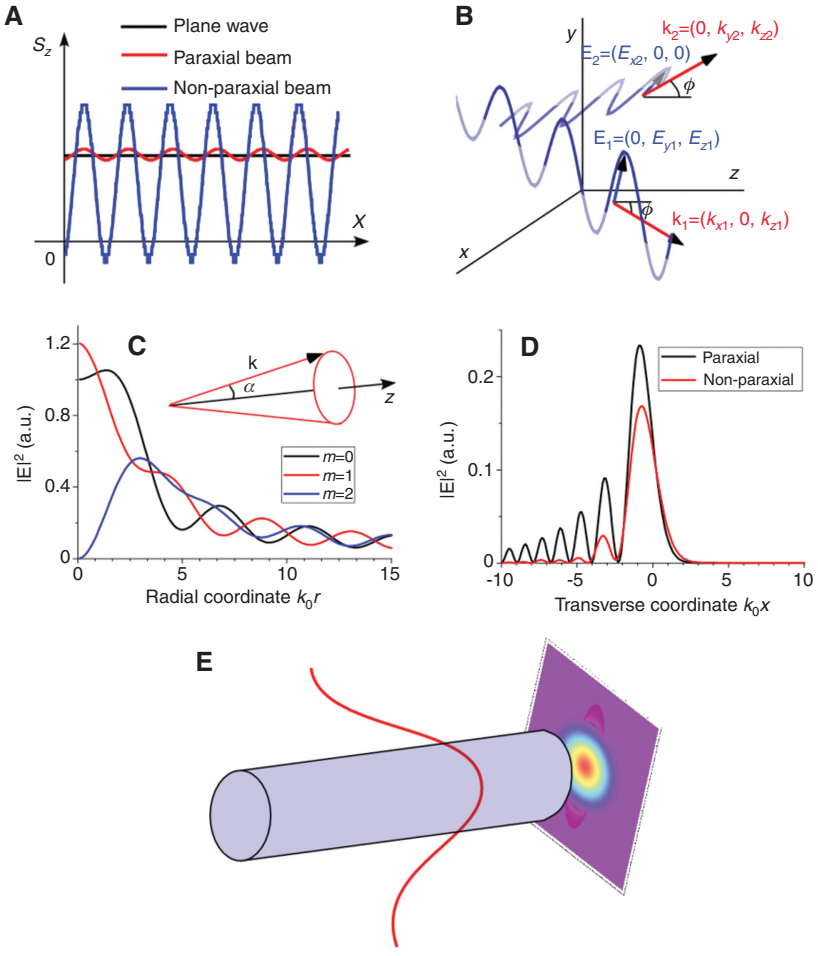

Figure 8 (A) Sketch illustrating possible Poynting vector component S_z for plane waves, paraxial beams and non-paraxial beams; (B) configuration of two plane waves resulting in the regions of negative component of Poynting vector $S_z(x, y, z)$; (C) squared electric field for non-paraxial Bessel beams of different orders m with the angle α=50° at the vertex of the cone in the spectrum of Bessel beam (shown in the inset); (D) paraxial and non-paraxial Airy beam profiles at the distance k_0z=0.5 from the source ($k_0=2\pi/\lambda$ is the wavenumber in vacuum). The paraxial beam maintains its intensity profile, while the non-paraxial Airy beam is disturbed; (E) schematic illustration of the fiber generating the regions of the negative Poynting vector components.

5.2 Negative Poynting vector

5.2.1 Plane waves

The simplest system to introduce the negative Poynting vector is a superposition of several plane waves. Actually, two plane waves are sufficient. In agreement with Ref. [105] we consider two plane waves as depicted in Figure 8B and detect the Poynting vector component in the z direction. The superposition of the plane waves results in sufficiently non-paraxial electromagnetic field, if the angle ϕ is large enough. From Figure 9 we notice that ϕ should be <45° to ensure the emergence of the reversed Poynting vector. On the other hand, small y-components of the electric field of the first plane wave are preferred. This means that the other (longitudinal) field component E_{z1} is responsible for the negative energy flux density of the superposition. Spatial distribution of the Poynting vector component in the inset of Figure 9 shows strong oscillations as we predicted before. Symmetric wave structures with respect to the z-axis are also possible and will be considered in the following subsection.

5.2.2 Bessel beams

When three-dimensional electromagnetic field consists of plane waves with wave vectors forming a cone (see the inset in Figure 8C), the field can form a Bessel light beam. Paraxial Bessel beams with small angles α at the vertex of the cone are well studied both theoretically and experimentally and their fascinating properties such as

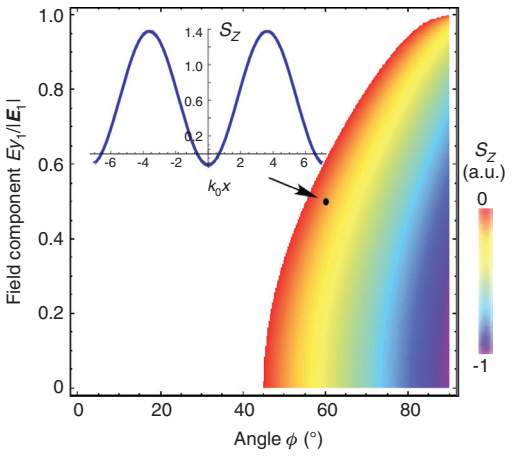

Figure 9 Negative $S_z(x=0, y=0, z=0)$, realized for various combinations of the angle ϕ and the electric field component E_{y1}. In the inset, $S_z(x, 0, 0)$ demonstrates the region of negative values for $\phi=60°$ and $E_{y1}=0.5\,|E_1|$.

non-diffraction propagation [108, 109] and self-reconstruction [110] are known. Non-paraxial Bessel beams are the full-vector solutions of the Maxwell equations and can be theoretically constructed for any angle at the cone vertex α. In contrast to the paraxial Bessel beams, their non-paraxial analog has not been studied much experimentally. Nevertheless, the non-paraxial Bessel beams possess amazing properties. First of all they are able to produce the regions of the reversed Poynting vector [106, 111].

In general, a non-paraxial Bessel beam consists of oppositely polarized components, TM and TE non-paraxial Bessel beams with complex amplitudes $c_1=|c_1|\exp(i\psi_1)$ and $c_2=|c_2|\exp(i\psi_2)$, respectively. Non-paraxial Bessel beams of different orders m are depicted in Figure 8C. Squared electric field of a non-paraxial Bessel beam is described by the Bessel functions. Only in paraxial approximation the Bessel beam of the mth order is defined by the Bessel function of the same order. In general, this is not the case [106]. Depending on the relative phase $\psi=\psi_1-\psi_2$ ($|c_1|=|c_2|=1$) and angle α, the Poynting vector component S_z is determined and shown in Figure 10. Although a negative Poynting vector component arises at the axis of the beam $r=0$ even for paraxial beams (α close to 0), it is hard to meet the appropriate conditions, because the TM and TE beams must be $\pi/2$-shifted with very sharp tolerance (Figure 10A). The largest effect of reversed Poynting vector exists for strongly non-paraxial Bessel beams. It should be noted that the regions of $S_z<0$ appear off the axis of the beam, too, as indicated in the insets of Figure 10 with the concentric rings. Therefore, the negative Poynting vector component as function of angles ψ and α can be found at $k_0r=3$, where k_0 is the wavenumber in vacuum. Note that despite the regions of negative Poynting vector components, the whole energy flux through the infinite plane z=const is positive.

Actually, any non-paraxial beam can be used to introduce locally negative energy flux density. We will mention only X-waves and Airy beams. An X-wave is weighted frequency superposition of Bessel beams, and it demonstrates all negative components of the Poynting vector. As mentioned in Ref. [112], a truncated X-wave can exhibit negative energy flux. Airy light beams [24, 113] had their precursors in quantum mechanics called non-spreading wave packets [114]. Airy beams received their name exactly owing to the similarity between the Schrödinger equation and the diffraction equation. They maintain their intensity during propagation (Figure 8D), but shift the distribution in the transversal direction, emulating the effect of

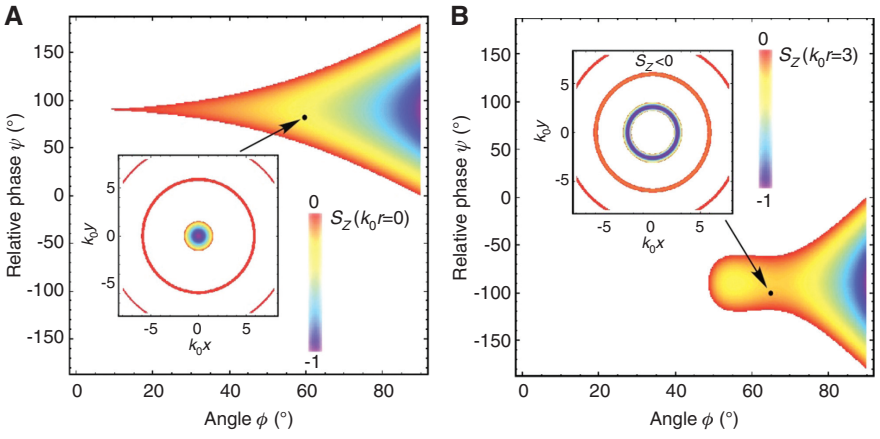

Figure 10 Diagrams of negative Poynting vector component S_z (in a.u.) of the first-order non-paraxial beams calculated at (A) $k_0r=0$ and (b) $k_0r=3$. In the insets, the negative component $S_z(x, y)$ for parameters (A) $\alpha=60°$ and $\psi=80°$, and (B) $\alpha=70°$ and $\psi=-100°$ is demonstrated.

an accelerated particle on a parabola. The non-paraxial Airy beam loses the property of non-diffraction. It is basically a superposition of propagating and evanescent field parts [115]. Superposition of propagating and evanescent components at the low-intensity fringes of the Airy function results in the negative S_z [116] and, unlike Bessel light beams, the superposition of the TE and TM beams is no longer needed. Thus, the evanescent field part of the Airy beam not only leads to the harmful spreading, but also engages the negative-Poynting effects.

6 Pulling optical force

6.1 Precursors of tractor beams

It has been almost three decades since the introduction and experimental observation of optical trap beam by Ashkin in 1986 [9]. After that, optical trapping and manipulation techniques, known as optical tweezers, have found applications in biological, physical, and chemical research [1, 2]. Using light to manipulate objects with high precision and finesse can revolutionize multidisciplinary research fields. This technique made it possible to reach lower temperatures in atomic cooling [117–119], to achieve higher resolution in light scattering [120], to manipulate living biological cells at will without causing damage [121–123], and to fabricate complex nanoscale structures [124].

Light has linear and angular momenta, which could exert forces and torques on small objects. The optical force had been verified in experiments at the beginning of 1900s. However, due to positive radiation pressure and momentum conservation, the forces usually push the object along the direction of the light [35]. Ashkin, one of the pioneers in optical trapping, reported the first experimental observation of stable trapping by using two opposing equal Gaussian beams [8]. The stable equilibrium was located at the symmetry point of the two beams. Particles exhibited a restoring force near the stable symmetry point, and would be trapped there. Subsequently, the trapping theory was developed and found numerous applications in optical levitation [125, 126].

In 1986, Ashkin and his co-workers proposed a single focused beam to trap small neutral particles by gradient force [9], which is the foundation of modern optical manipulation techniques. Small particles in the electric field of light develop an electric dipole moment that can be described by the induced polarizability α. The induced electric dipole of high refractive index particles undertakes a gradient force $(1/2)\alpha\nabla\boldsymbol{E}^2$ toward the beam focus. Meanwhile, the particle suffers from the scattering force, which originates from the momentum transferred to the particle from the incident beam and points along its direction. When the gradient force overwhelms the scattering force, small particles can be firmly trapped near the focal point, and the particles can also be manipulated in three dimensions by changing the location of the beam focus.

6.2 Poynting-vector indicators of pulling force

The simplest system to show the appearance of the pulling force effect in the field of a gradientless beam is a small (Rayleigh-limit) spherical particle. Non-magnetic Rayleigh beads in inhomogeneous field $\boldsymbol{E}=g(z)\exp(ik_z z)\mathbf{e}$ are affected by the time-averaged force

$$F_z=\frac{\varepsilon_0|\boldsymbol{e}|^2}{2}\left(\frac{\mathrm{Re}(\alpha_e)}{2}\frac{d(g^2)}{dz}+k_z g^2\,\mathrm{Im}(\alpha_e)\right), \tag{6.1}$$

where α_e is the relative electric polarizability of the particle. The first term is the gradient force and the second one is the nonconservative force. Usually the gradient force is dominant and can serve for quite effective optical manipulation in optical tweezers. Indeed, the positive and negative gradient of the field is able to pull and push particles. Using spatial modulation techniques, it is feasible to move the nanoparticles along arbitrary trajectories.

When there is no gradient of the electric field, i.e., $g(z)$ is constant function, we lose control over the bead's axial movement and we get a unidirectional force, which can push transparent and lossy particles and pull spheres with optical gain [39]. We are interested in the approaches to achieve pulling of transparent and lossy beads using gradientless electromagnetic fields without resorting to quite exotic gain particles.

Let us start by considering magnetic spherical particles of radius R, relative dielectric permittivity ε and magnetic permeability μ. We assume that Rayleigh particles are electromagnetically small, so the condition $\sqrt{\varepsilon\mu}R/\lambda<<1$ is fulfilled. The beads possess induced electric $\boldsymbol{p}$ and magnetic $\boldsymbol{m}$ dipole moments, which depend on the incident electric $\mathbf{E}$ and magnetic $\boldsymbol{H}$ fields at the center of the sphere, and electric α_e and magnetic α_m polarizabilities as $\boldsymbol{p}=\varepsilon_0\alpha_e\boldsymbol{E}$ and $\boldsymbol{m}=\alpha_m\boldsymbol{H}$, respectively. In the Rayleigh approximation, the total polarizabilities are expressed in terms of the static polarizabilities $\alpha_{e,m}^{(0)}$:

$$\alpha_{e,m}=\frac{4\pi\alpha_{e,m}^{(0)}}{1-i\frac{2}{3}k_0^3\alpha_{e,m}^{(0)}},\qquad \alpha_e^{(0)}=R^3\frac{\varepsilon-1}{\varepsilon+2},\qquad \alpha_m^{(0)}=R^3\frac{\mu-1}{\mu+2}. \quad (6.2)$$

Localized plasmonic resonance arises for $\varepsilon=-2$ ($\mu=-2$), but far from resonance the inequality $|\mathrm{Re}(\alpha_{e,m})|>>\mathrm{Im}(\alpha_{e,m})$ holds for small nanoparticles. For transparent (non-absorbing) beads the permittivities and permeabilities are real, as static polarizabilities.

The time-averaged component of the force along the optical axis of the beam z has the form [42]

$$F_z=\frac{1}{2}\left[\varepsilon_0\,\mathrm{Re}\left(\alpha_e\boldsymbol{E}\frac{\partial\boldsymbol{E}^*}{\partial z}\right)+\mu_0\,\mathrm{Re}\left(\alpha_m\boldsymbol{H}\frac{\partial\boldsymbol{H}^*}{\partial z}\right)\right] -\frac{k_0^4}{12\pi c}\mathrm{Re}(\alpha_e\alpha_m^*[\boldsymbol{E}\times\boldsymbol{H}^*]_z). \quad (6.3)$$

Propagation-invariant (non-diffractive) light beams have the same intensity pattern for any z, i.e., $\boldsymbol{E}=\boldsymbol{e}(\mathbf{r}_\perp)\exp(i\beta k_0 z)$, where $\mathbf{r}_\perp=\mathbf{r}-z\mathbf{e}_z$ is the transverse radius-vector and $\beta=(\boldsymbol{e}_z\boldsymbol{k})$ is the longitudinal component of the wavevector (propagation constant). Propagation-invariant beams do not exert gradient forces on the beads in the z-direction, so the same nonconservative force can affect the particle for a long time. The condition $\mathrm{Re}(\alpha_{e,m})>>\mathrm{Im}(\alpha_{e,m})$ allows us to simplify the last term in the expression for the force (6.3) as $\mathrm{Re}(\alpha_e\alpha_m^*[\boldsymbol{E}\times\boldsymbol{H}^*]_z)\approx\mathrm{Re}(\alpha_e)\,\mathrm{Re}(\alpha_m)\,\mathrm{Re}([\boldsymbol{E}\times\boldsymbol{H}^*]_z)$. Thus, one rewrites Eq. (6.3) as

$$F_z=\frac{k_0\beta}{2}[\varepsilon_0\,\mathrm{Im}(\alpha_e)|\boldsymbol{E}|^2+\mu_0\,\mathrm{Im}(\alpha_m)|\boldsymbol{H}|^2] -\frac{k_0^4}{6\pi c}\mathrm{Re}(\alpha_e)\,\mathrm{Re}(\alpha_m)S_z. \quad (6.4)$$

The first two terms proportional to the imaginary parts of the polarizabilities are always positive for transparent and absorptive particles. For paraxial propagation-invariant electromagnetic beams these positive terms are much larger than the third term, so the resulting force is always pushing. The sign of the third term in Eq. (6.4) depends on the sign of the longitudinal component of the Poynting vector S_z. When $\mathrm{Re}(\alpha_e)\mathrm{Re}(\alpha_m)>0$, the nanoparticle can experience a pulling force in the region of positive S_z, but only if S_z is large and β is small enough. The requirement of small longitudinal component of the wavevector β means that the wavevectors of partial plane waves form large angles with respect to the axis z or, in other words, the beam is strongly non-paraxial. Non-paraxial beams are generally needed to create the reversed Poynting vector effect, too, but in this case $S_z<0$ is not required. On the contrary, the regions with positive Poynting vector components are preferred. Condition on the polarizabilities $\mathrm{Re}(\alpha_e)\mathrm{Re}(\alpha_m)>0$ is valid for transparent beads, when ($\varepsilon<-2$ or $\varepsilon>1$) and ($\mu<-2$ or $\mu>1$), or $1>\varepsilon>-2$ and $1>\mu>-2$.

On the other hand, nanoparticles are also pulled towards the light source when $\mathrm{Re}(\alpha_e)\mathrm{Re}(\alpha_m)<0$, the Poynting vector component S_z is negative, and β is small. This case corresponds to the beads made of a metamaterial with rather non-conventional permittivities and permeabilities: either ($\varepsilon<-2$, $\varepsilon>1$) and $1>\mu>-2$, or $1>\varepsilon>-2$ and ($\mu<-2$, $\mu>1$). Figure 11 demonstrates the optical pulling forces in the cases of positive and negative Poynting vector component S_z.

How small longitudinal wavenumber β should be can be estimated for the non-absorptive Rayleigh nanoparticles with $\mathrm{Re}(k_0^3\alpha_{e,m})=4\pi\alpha_{e,m}^{(0)}$ and $\mathrm{Im}(k_0^3\alpha_{e,m})=8\pi\alpha_{e,m}^{(0)2}/3$. The force (6.4) is pulling, if

$$\beta<\frac{k_0^3\,\mathrm{Re}(\alpha_e)\,\mathrm{Re}(\alpha_m)S_z}{6\pi\sqrt{\mathrm{Im}(\alpha_e)\,\mathrm{Im}(\alpha_m)}\,|\boldsymbol{E}||\boldsymbol{H}|} \quad (6.5)$$

Using the inequality $\mathrm{Re}(\boldsymbol{E}\times\boldsymbol{H}^*)_z<|\boldsymbol{E}||\boldsymbol{H}|$, one derives $\beta<1/2$. Introducing the angle $\alpha=\arccos(\beta)$, which forms a partial plane wave with respect to the $z$axis (it is the angle at the vertex of the cone for Bessel beams), we estimate its value as $\alpha>60°$. This clearly means that the light beam should be strongly nonparaxial to pull a small sphere. When the sphere is lossy, α should be even greater.

The effect of pulling force can be understood both from the wave and from the corpuscular point of view. The stream of photons incident on a bead creates two contributions to the optical force [31]. The first one is interpreted as direct transfer of the longitudinal momentum $\hbar k_0\beta$ of

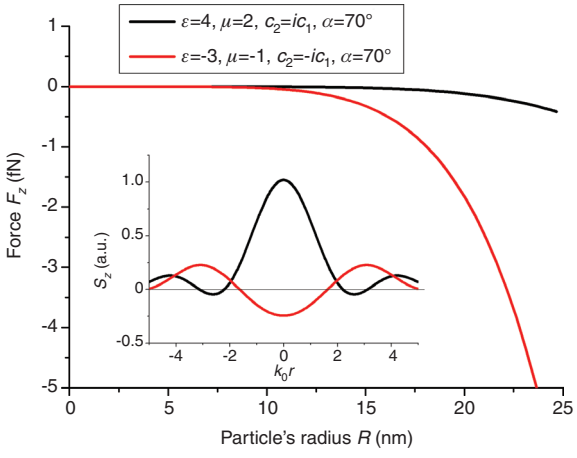

Figure 11 Pulling optical force at the axis of the beam $r=0$, when the Poynting vector is (A) positive and (B) negative. Parameters: $c_1=10^8$ V/m, $\lambda=1.55$ μm. The Poynting vector of the non-paraxial Bessel light beam of the first order is depicted in the inset.

the incident photons to nanoparticles. The second contribution takes into account the effect of scattered photons. If the photons are primarily backscattered, they transfer positive momentum to the bead according to the momentum conservation law. Then the particle is pushed by the incident beam like it happens in paraxial beams. When the angle α is large (non-paraxial beam), the forward scattering increases and the transferred momentum becomes negative – the particle is pulled by a propagation invariant light beam! This situation can be noticed in the diagrams of differential cross-sections, i.e., in the far-zone characteristics of scattering. In Figure 12 we notice that forward scattering exceeding backward scattering is in fact the defining characteristic of the pulling force. However, this approach does not predict the exact value of the critical angle α, which should be at least 60°. Even though the optical force and the difference between forward- and backward-scattering cross-sections both stem from the expressions similar to the third term in Eq. (6.3), they are not simply proportional. So, the qualitative indicator of the pulling force is the scattering pattern. It should be noted that the analogous explanation for the negative force was made for acoustic Bessel beams in Refs. [33, 127, 128].

The second interpretation of the negative-force effects is based on the multipole approach [31, 35, 38]. Eq. (6.3) is the force written with only electric and magnetic dipole moments. This means that in the case of Rayleigh particles we can be limited by only several terms of the series, which generally includes also quadrupole terms, octupole terms, etc. The effect of the pulling force appears owing to the interaction of these multipoles. Say, in Eq. (6.3) the third term describes the interaction between the electric ($\boldsymbol{p}$) and the magnetic ($\boldsymbol{m}$) dipole moments and is proportional to Re($\boldsymbol{p}\times\boldsymbol{m}^*$). Thus, the series can be presented in the form

$$\boldsymbol{F}=\boldsymbol{F}_d+\boldsymbol{F}_q+\boldsymbol{F}_o+\ldots \tag{6.6}$$

$\boldsymbol{F}_d$ consists of positive dipole inputs and a dipole-interaction term, which can be either positive or negative. $\boldsymbol{F}_q$ is the quadrupole terms and electric-magnetic quadrupole and quadrupole-dipole interaction terms. $\boldsymbol{F}_o$ includes the interaction of octupoles with dipoles, quadrupoles, and octupoles themselves.

Eq. (6.6) should be applied for large Mie particles. The polarizabilities for large particles can be presented as in Eq. (6.2), but the static polarizabilities should be replaced by different quantities, expressed in terms of the spherical Bessel functions (first Mie coefficients a_1 and b_1). With these non-static polarizabilities the force (6.3) can be used for much larger particles. One more good issue is that magnetic permeability is no longer needed to achieve the pulling force effect. One can use the artificial magnetic permeability [129, 130] instead, which stems from the dielectric permittivity in the Mie coefficient b_1. Taking a non-magnetic polystyrene bead, e.g., the dipole approximation correctly predicts the appearance of the

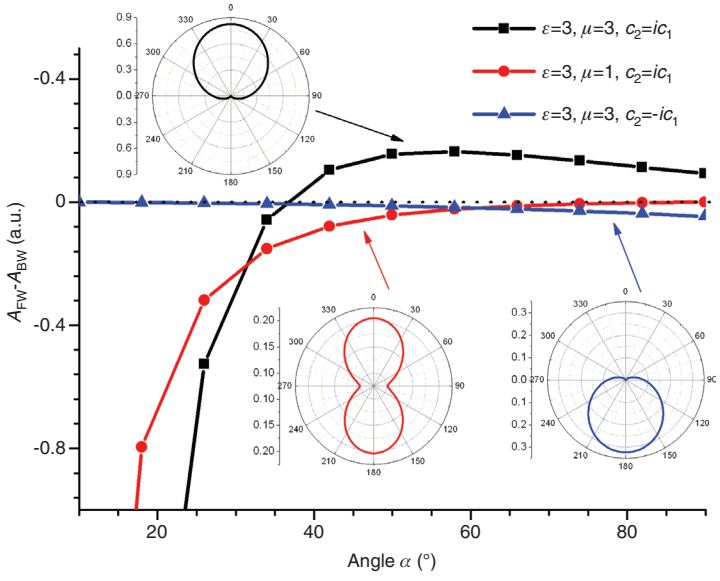

Figure 12 Difference between forward- and backward-scattering cross-sections calculated as $\int_0^{\alpha}(d\sigma/do)d\theta-\int_{\alpha}^{\pi}(d\sigma/do)d\theta$ *vs.* the angle α of the non-paraxial Bessel beam. Differential cross-sections are shown in the insets. Parameters: λ=532 nm, R=8.5 nm, m=1.

pulling force effect near the electric size k_0R=1.4, but fails for larger particles. Both dipole and quadrupole terms (including their interaction) are sufficient to describe the pulling force effect in the size up to k_0R=3.5.

It should also be noted that the near-field Poynting vector mapping alone is not able to predict the dynamics of the object in the light field. One needs to apply the integration of the Maxwell stress tensor over the surface around the object. This exact formula is transformed into the integration of the Poynting vector only at the infinite radius of the integration sphere, resulting in the expression $\boldsymbol{F}=-(1/c)\oint(\boldsymbol{S}-\boldsymbol{S}_{inc})ds$, where $\boldsymbol{S}$ and $\boldsymbol{S}_{inc}$ are the Poynting vectors of the total field (including scattering) and incident field, respectively. When the integration is performed over finite spheres, the force cannot be calculated in terms of the energy flux density. If we use the aforementioned formula based on the Poynting vector nonetheless, we get oscillations depending on the radius of the integration. The correct value is achieved only at infinity or by means of the averaging over a large number of oscillations. In the latter case, calculation of the optical force is reduced to integration over the radial coordinate, i.e., we get to the expression for the force in the form of the Newton's law of dynamics $\boldsymbol{F}=\Delta\boldsymbol{G}/\Delta t$, where $\Delta\boldsymbol{G}=(1/c^2)\int(\boldsymbol{S}_{inc}-\boldsymbol{S})dV$ is the momentum transferred to the bead from the electromagnetic field. The integration should be carried out over the infinite surface to obtain the exact result. When the integration embraces only finite volume, the force is still oscillatory, but the amplitude of such oscillations is suppressed.

6.3 Solenoid tractor beams and optical conveyors

The experimental demonstration of optical tractor beams has been realized, among others, by theoptical solenoid, which draws colloidal silica spheres against the light's direction of propagation [26]. The total force is the combination of intensity gradient force (drawing particles to the intensity maximum) and phase gradient force (pushing particles along the light axis). By variation of helical pitch of solenoid beam, the phase-gradient forces can be manipulated to transport particles in both directions of the optical axis. Theoretically, solenoid beams are diffraction-free [82], but the trapping extents are limited by optical system. Due to the interference of the projected solenoid beam and higher diffraction orders, the intensity of solenoid beam is actually not uniform along the solenoid, hence the particle will be localized somewhere along the solenoid.

Solenoid beams can also work as optical conveyors, making objects move back and forth. The pulling distance is increased greatly by using a coaxial Bessel beam [37, 131]. Moreover, despite the variations in geometrical or optical properties of the particles, they can be trapped continuously at a stable speed. Simply changing the phase variation rate along the conveyors could move the object in the other direction, making it a bidirectional optical conveyor [37].

6.4 Manipulation by interfering optical fields

Compared to gradient force, trapping forces from gradientless light beams show many advantages in controlling objects, such as long range trapping. In the view of momentum conservation, two situations are favorable for getting optical pulling force. One is to concentrate the scattering in the forward direction, as was described above. The other is to try and impart less momentum along the propagation direction of light. When the forward scattering overwhelms the photon momentum in the propagation direction, an object could be drawn towards the light source.

Kerker et al. [132] predicted that backward scattering of a small dielectric sphere becomes zero when its parameters satisfy the condition $\varepsilon=\mu$. For a Rayleigh sphere, the light scattering can be approximated by the dipole terms of the Mie expansion. Then the scattered intensities are reduced to very simple forms to obtain the conditions for zero backward scattering and zero forward scattering. Though there are some exceptions to the Kerker theory [133, 134], this prediction was confirmed experimentally in the microwave range [135]. Increasing the particle size, higher-order multipoles could appear and interact with the dipole mode, giving rise to a Fano resonance [136]. Around the Fano resonance, the backward scattering and forward scattering spectra have asymmetric shapes. At the dip of backward scattering, the light scattering could also be focused in the forward direction [136]. In both these cases, the optical pushing forces are considerably reduced [137, 138]. However, a plane wave still cannot exert a pulling force on a dielectric sphere because scattering cannot fully occur in the forward direction.

Compared to a plane wave, the wave vector of Bessel beam is not in the propagating direction, but with an angle θ_0 which could be controlled to impart less incident momentum in the direction of wave propagation. Chen et al. realized an optical pulling force by maximizing the forward

scattering, which is due to the coupling between radiation multipoles, and at the same time by keeping the projection of photon momentum along the propagation axis small. The total z-component of the force for a lossless particle includes an incident part and an interference part [31],

$$F_z = F_z^{\text{incident}} + F_z^{\text{interference}} = W_{\text{sca}} c^{-1} (\cos\theta_0 - \langle \cos\theta \rangle) \tag{6.7}$$

where W_{sca} is the energy scattering rate, and $\langle \cos\theta \rangle$ represents the averaged cosine of the scattering angle, which depends on the properties of the particles and the incident beam. It also reflects the interference between the particle and incident beam, and can be tuned by the phases in the multipoles. When $\langle \cos\theta \rangle$ is larger than $\cos\theta_0$, the total force will pull the particle back to the light source. Note that a Bessel beam without a phase shift between its TE and TM components could also show negative forces as long as the excited electric moments are greater than the excited magnetic moments [35]. $\pi/2$ phase-shifted beams are found to have wider ranges of material parameter for the existence of pulling force. The negative force region is almost symmetric in the force diagram of permittivity versus permeability. Meanwhile, particles satisfying the Kerker condition of zero-backward scattering are more favorable for optical trapping.

So far, the pulling force of a Bessel beam has been sensitive to the particle size and material parameters. Further study revealed that optical tractor beam could pull dipole objects almost of any size and refractive index [34]. The force on a dipole particle can be written as Eq.(6.4). The first two terms in that equation represent the contributions from the electric dipole and the magnetic dipole. The third term is the interaction between these two dipoles, which is the origin of negative force. To obtain a pulling force, small k_z and large P_z are required. This means the Bessel beam should be strongly nonparaxial ($\theta_0 > 60°$) to realize universal pulling. In spite of considerable challenges in generation of such strongly nonparaxial Bessel beams, the hypergeometric laser beam [139] is a promising candidate to possess the required nonparaxiality. On the other hand, the scattered field can be focused in the forward direction by controlling the interaction of the electric and magnetic dipoles. Then the optical force on the dipole particle is negative due to the momentum conservation and can pull the particle as a tractor beam. Very recently, tractor beams have been demonstrated experimentally to move, transport, and sort various sizes of spherical particles [36]. The works on the interference between the particles and light field will provide deep insights on the light-matter interaction and extend the similar ideas to acoustics [34, 140].

7 Conclusions

We have provided an overview of various principles governing the interaction between light and microparticles. These principles help identify the available degrees of freedom for engineering light-matter interaction to enable and widen the emerging applications of optical micromanipulation. Understanding the intricate light-matter interaction from the use of synthesized complex electromagnetic beams and/or designed micro- and nano-structured objects can be useful for achieving desired light scattering or exploit the phase gradient and angular momentum of the light. In particular, we reviewed the optical manipulation of synthesized microstructures, which is enabling new possibilities in force sensing and light delivery. We also reviewed some propagation-invariant beams and accelerating beams such as Bessel and Airy beams which have infinite energy and do not diffract. They possess the self-healing property, i.e., reconstructing the beam after the interaction with an obstacle. Interesting properties arise for non-paraxial Bessel beams whose plane wave components form large angles with respect to the optical axis. The Poynting vector of the non-paraxial Bessel beams can be locally reversed, thus inducing speculations about the pulling microobjects to the light source. Actually, reversed energy flux density is not a rare phenomenon: it appears for any non-paraxial beam, as well as in an optical fiber. Though the reversed Poynting vector does not result in the pulling optical force, the latter emerges for non-paraxial Bessel beams owing to the multipoles interaction. Together with the ordinary tweezers technique, non-paraxial beams can be applied for the optical manipulation acting on particle as a tractor beam. The concepts we considered have the general wave nature and, therefore, may be applicable for optic and acoustic beams.

Acknowledgments: CWQ acknowledges the support by National University of Singapore (Grant No. R-263-000-678-133). JG and DP thank the support from the Danish Strategic Research Council.

Received December 2, 2013; accepted March 25, 2014; previously published online April 11, 2014

References

[1] Ashkin A. History of optical trapping and manipulation of small-neutral particle, atoms, and molecules. IEEE J Sel Top Quant 2000;6:841–56.

[2] Grier DG. A revolution in optical manipulation. Nature 2003;424:810–6.

[3] Moffitt JR, Chemla YR, Smith SB, Bustamante C. Recent advances in optical tweezers. Annu Rev Biochem 2008;77:205–28.

[4] Schuller JA, Barnard ES, Cai WS, Jun YC, White JS, Brongersma ML. Plasmonics for extreme light concentration and manipulation. Nat Mater 2010;9:193–204.

[5] Kepler J. Ad vitellionem parali pomena. Frankfort 1604.

[6] Kepler J. De cometis liballi tres. *Augsburg* 1619.

[7] Maxwell JC. A dynamical theory of the electromagnetic field. Philos Tr R Soc 1865;155:459–512.

[8] Ashkin A. Acceleration and trapping of particles by radiation pressure. Phys Rev Lett 1970;24:156–9.

[9] Ashkin A, Dziedzic JM, Bjorkholm JE, Chu S. Observation of a single-beam gradient force optical trap for dielectric particles. Opt Lett 1986;11:288–90.

[10] Metzger NK, Wright EM, Sibbett W, Dholakia K. Visualization of optical binding of microparticles using a femtosecond fiber optical trap. Opt Express 2006;14:3677–87.

[11] Reece PJ, Garces-Chavez V, Dholakia K. Near-field optical micromanipulation with cavity enhanced evanescent waves. Appl Phys Lett 2006;88. [doi: 10.1063/1.2208272].

[12] Juan ML, Gordon R, Pang YJ, Eftekhari F, Quidant R. Self-induced back-action optical trapping of dielectric nanoparticles. Nat Phys 2009;5:915–9.

[13] Grigorenko AN, Roberts NW, Dickinson MR, Zhang Y. Nanometric optical tweezers based on nanostructured substrates. Nat Photon 2008;2:365–70.

[14] Grzegorczyk TM, Kemp BA, Kong JA. Stable optical trapping based on optical binding forces. Phys Rev Lett 2006;96:113903.

[15] Righini M, Ghenuche P, Cherukulappurath S, Myroshnychenko V, de Abajo FJG, Quidant R. Nano-optical trapping of rayleigh particles and Escherichia coli bacteria with resonant optical antennas. Nano Lett 2009;9:3387–91.

[16] Swartzlander GA, Peterson TJ, Artusio-Glimpse AB, Raisanen AD. Stable optical lift. Nat Photon 2011;5:48–51.

[17] Roichman Y, Sun B, Roichman Y, Amato-Grill J, Grier DG. Optical forces arising from phase gradients. Phys Rev Lett 2008;100:013602.

[18] Li M, Pernice WHP, Tang HX. Tunable bipolar optical interactions between guided lightwaves. Nat Photon 2009;3:464–8.

[19] Wiederhecker GS, Chen L, Gondarenko A, Lipson M. Controlling photonic structures using optical forces. Nature 2009;462:633–U103.

[20] Shvedov VG, Rode AV, Izdebskaya YV, Desyatnikov AS, Krolikowski W, Kivshar YS. Giant optical manipulation. Phys Rev Lett 2010;105:118103.

[21] Amaral AM, Falcão-Filho EL, de Araújo CB. Shaping optical beams with topological charge. Opt Lett 2013;38:1579–81.

[22] Padgett M, Bowman R. Tweezers with a twist. Nat Photon 2011;5:343–8.

[23] Mazilu M, Stevenson DJ, Gunn-Moore F, Dholakia K. Light beats the spread: non-diffracting beams. Laser Photon Rev 2010;4:529–7.

[24] Siviloglou GA, Broky J, Dogariu A, Christodoulides DN. Observation of accelerating Airy beams. Phys Rev Lett 2007;99:213901.

[25] Hermosa N, Rosales-Guzmán C, Torres JP. Helico-conical optical beams self-heal. Opt Lett 2013;38:383–5.

[26] Lee SH, Roichman Y, Grier DG. Optical solenoid beams. Opt Express 2010;18:6988–93.

[27] Zhang DW, Yuan XC. Optical doughnut for optical tweezers. Opt Lett 2003;28:740–2.

[28] Asavei T, Loke VLY, Barbieri M, Nieminen TA, Heckenberg NR, Rubinsztein-Dunlop H. Optical angular momentum transfer to microrotors fabricated by two-photon photopolymerization. New J Phys 2009;11:093021.

[29] Maruo S, Takaura A, Saito Y. Optically driven micropump with a twin spiral microrotor. Opt Express 2009;17:18525–32.

[30] Wu T, Nieminen TA, Mohanty S, Miotke J, Meyer RL, Rubinsztein-Dunlop H, Berns MW. A photon-driven micromotor can direct nerve fibre growth. Nat Photon 2012;6:62–7.

[31] Chen J, Ng J, Lin ZF, Chan CT. Optical pulling force. Nat Photon 2011;5:531–4.

[32] Sukhov S, Dogariu A. On the concept of 'tractor beams'. Opt Lett 2010;35:3847–9.

[33] Marston PL. Axial radiation force of a Bessel beam on a sphere and direction reversal of the force. J Acoust Soc Am 2006;120:3518–24.

[34] Novitsky A, Qiu CW, Lavrinenko A. Material-Independent and Size-independent tractor beams for dipole objects. Phys Rev Lett 2012;109:023902.

[35] Novitsky A, Qiu C-W, Wang H. Single gradientless light beam drags particles as tractor beams. Phys Rev Lett 2011;107:203601.

[36] Brzobohatý O, Karásek V, Šiler M, Chvátal L, Čižmár T, Zemánek P. Experimental demonstration of optical transport, sorting and self-arrangement using a'tractor beam'. Nat Photon 2013;7:123–7.

[37] Ruffner DB, Grier DG. Optical conveyors: a class of active tractor beams. Phys Rev Lett 2012;109:163903.

[38] Sukhov S, Dogariu A. Negative nonconservative forces: optical 'Tractor Beams' for arbitrary objects. Phys Rev Lett 2011;107:203602.

[39] Mizrahi A, Fainman Y. Negative radiation pressure on gain medium structures. Opt Lett 2010;35:3405–7.

[40] Webb KJ, Shivanand. Negative electromagnetic plane-wave force in gain media. Phys Rev E 2011;84. [doi: 10.1103/PhysRevE.84.057602].

[41] Salandrino A, Christodoulides DN. Reverse optical forces in negative index dielectric waveguide arrays. Opt Lett 2011;36:3103–5.

[42] Nieto-Vesperinas M, Sáenz JJ, Gómez-Medina R, Chantada L. Optical forces on small magnetodielectric particles. Opt Express 2010;18:11428–43.

[43] Farré A, Montes-Usategui M. A force detection technique for single-beam optical traps based on direct measurement of light momentum changes. Opt Express 2010;18:11955–68.

[44] Zakharian AR, Polynkin P, Mansuripur M, Moloney JV. Single-beam trapping of micro-beads in polarized light: numerical simulations. Opt Express 2006;14:3660–76.
[45] Pralle A, Prummer M, Florin EL, Stelzer EHK, Hörber JKH. Three-dimensional high-resolution particle tracking for optical tweezers by forward scattered light. Microsc Res Tech 1999;44:378–86.
[46] Smith SB, Cui Y, Bustamante C. Optical-trap force transducer that operates by direct measurement of light momentum. In: Gerard M, Ian P, eds. Methods in Enzymology. Academic Press; 2003. pp. 134–162.
[47] Nieminen TA, Loke VLY, Stilgoe AB, Knöner G, Brańczyk AM, Heckenberg NR, Rubinsztein-Dunlop H. Optical tweezers computational toolbox. J Opt A, Pure Appl Opt 2007;9: S196–203.
[48] Simpson SH, Hanna S. Application of the discrete dipole approximation to optical trapping calculations of inhomogeneous and anisotropic particles. Opt Express 20011;19:16526–41.
[49] White DA. Numerical modeling of optical gradient traps using the vector finite element method. J Comp Phys 2000;159: 13–37.
[50] Hoekstra AG, Frijlink M, Waters LBFM, Sloot PMA. Radiation forces in the discrete-dipole approximation. J Opt Soc Am A 2001;18:1944.
[51] Harada Y, Asakura T. Radiation forces on a dielectric sphere in the Rayleigh scattering regime. Opt Commun 1996;124: 529–41.
[52] Rohrbach A, Stelzer EHK. Optical trapping of dielectric particles in arbitrary fields. J Opt Soc Am A 2001;18:839–3.
[53] Ashkin A. Forces of a single-beam gradient laser trap on a dielectric sphere in the ray optics regime. Biophys J 1992;61:569–82.
[54] Loudon R, Baxter C. Contributions of John Henry Poynting to the understanding of radiation pressure. Proc R Soc A 2012;468:1825–38.
[55] Chaumet PC, Nieto-Vesperinas M. Time-averaged total force on a dipolar sphere in an electromagnetic field. Opt Lett 2000;25:1065–7.
[56] Ulriksen HU, Thøgersen J, Keiding SR, Perch-Nielsen IR, Dam JS, Palima DZ, Stapelfeldt H, Glückstad J. Independent trapping, manipulation and characterization by an all-optical biophotonics workstation. J Europ Opt Soc Rap Public 2008;3 [doi: 08034 10.2971/jeos.2008.08034].
[57] MacDonald MP, Spalding GC, Dholakia K. Microfluidic sorting in an optical lattice. Nature 2003;426:421–4.
[58] Ladavac K, Kasza K, Grier DG. Sorting mesoscopic objects with periodic potential landscapes: Optical fractionation. Phys Rev E 2004;70:010901.
[59] Jákl P, Cizmar T, Sery M, Zemánek P. Static optical sorting in a laser interference field. Appl Phys Lett 2008;92:161110-161110-161113.
[60] Mahamdeh M, Campos CP, Schäffer E. Under-filling trapping objectives optimizes the use of the available laser power in optical tweezers. Opt Express 2011;19:11759–68.
[61] Jannasch A, Demirlörs AF, van Oostrum PDJ, van Blaaderen A, Schäffer E. Nanonewton optical force trap employing anti-reflection coated, high-refractive-index titania microspheres. Nat Photonics 2012;6:469–73.
[62] Lindballe TB, Kristensen MVG, Berg-Sørensen K, Keiding SR, Stapelfeldt H. Pulsed laser manipulation of an optically trapped bead: averaging thermal noise and measuring the pulsed force amplitude. Opt Express 2013;21:1986–96.
[63] Palima D, Bañas AR, Vizsnyiczai G, Kelemen L, Ormos P, Glückstad J. Wave-guided optical waveguides. Opt Express 2012;20:2004–14.
[64] Palima D, Bañas AR, Vizsnyiczai G, Kelemen L, Aabo T, Ormos P, Glückstad J. Optical forces through guided light deflections. Opt Express 2013;21:581–93.
[65] Galajda P, Ormos P. Complex micromachines produced and driven by light. In: Lasers and Electro-Optics, 2002. CLEO'02. Technical Digest. Summaries of Papers Presented at the, pp. 634–5, IEEE (2002).
[66] Dholakia K, Čižmár T. Shaping the future of manipulation. Nat Photon 2011;5:335–42.
[67] Liberale C, Minzioni P, Bragheri F, De Angelis F, Di Fabrizio E, Cristiani I. Miniaturized all-fibre probe for three-dimensional optical trapping and manipulation. Nat Photon 2007;1:723–7.
[68] Čižmár T, Dholakia K. Shaping the light transmission through a multimode optical fibre: complex transformation analysis and applications in biophotonics. Opt Express 2011;19:18871–4.
[69] Čižmár T, Mazilu M, Dholakia K. In situ wavefront correction and its application to micromanipulation. Nat Photon 2010;4:388–94.
[70] Hart SJ, Terray A, Arnold J, Leski TA. Sample concentration using optical chromatography. Opt Express 2007;15:2724–31.
[71] Unterkofler S, Garbos MK, Euser TG, Russell PSJ. Long-distance laser propulsion and deformation-monitoring of cells in optofluidic photonic crystal fiber. J Biophoton 2012 [doi: 10.1002/jbio.201200180].
[72] Tauro S, Bañas A, Palima D, Glückstad J. Dynamic axial stabilization of counter-propagating beam-traps with feedback control. Opt Express 2010;18:18217–22.
[73] Glückstad J. Phase contrast image synthesis. Opt Commun 1996;130:225–30.
[74] Glückstad J, Mogensen PC. Optimal phase contrast in common-path interferometry. Appl Opt 2001;40:268–82.
[75] O'Neil AT, MacVicar I, Allen L, Padgett MJ. Intrinsic and extrinsic nature of the orbital angular momentum of a light beam. Phys Rev Lett 2002;88:053601.
[76] Shanblatt ER, Grier DG. Extended and knotted optical traps in three dimensions. Opt Express 2011;19:5833–8.
[77] Turunen J, Friberg AT. Propagation-invariant optical fields. Prog Opt 2010;54:1–88.
[78] Cottrell DM, Craven JM, Davis JA. Nondiffracting random intensity patterns. Opt Lett 2007;32:298–300.
[79] Dudley A, Vasilyeu R, Belyi V, Khilo N, Ropot P, Forbes A. Controlling the evolution of nondiffracting speckle by complex amplitude modulation on a phase-only spatial light modulator. Opt Commun 2012;285:5–12.
[80] López-Mariscal C, Helmerson K. Shaped nondiffracting beams. Opt Lett 2010;35:1215–7.
[81] Arlt J, Dholakia K. Generation of high-order Bessel beams by use of an axicon. Opt Commun 2000;177:297–301.
[82] Durnin J, Miceli JJ Jr., Eberly JH. Diffraction-free beams. Phys Rev Lett 1987;58:1499–501.
[83] Baumgartl J, Mazilu M, Dholakia K. Optically mediated particle clearing using Airy wavepackets. Nat Photon 2008;2:675–8.

[84] Daria VR, Palima DZ, Glückstad J. Optical twists in phase and amplitude. Opt Express 2011;19:476–81.
[85] Piestun R, Schechner YY, Shamir J. Propagation-invariant wave fields with finite energy. J Opt Soc Am A 2000;17:294–303.
[86] Bandres MA. Accelerating parabolic beams. Opt Lett 2008;33:1678–80.
[87] Broky J, Siviloglou GA, Dogariu A, Christodoulides DN. Self-healing properties of optical Airy beams. Opt Express 2008;16:12880–91.
[88] Paterson C, Smith R. Helicon waves: propagation-invariant waves in a rotating coordinate system. Opt Commun 1996;124:131–40.
[89] Rop R, Litvin IA, Forbes A. Generation and propagation dynamics of obstructed and unobstructed rotating orbital angular momentum-carrying helicon beams. J Opt 2012;14:035702.
[90] Alonzo CA, Rodrigo PJ, Glückstad J. Helico-conical optical beams: a product of helical and conical phase fronts. Opt Express 2005;13:1749–60.
[91] Maruo S, Fourkas JT. Recent progress in multiphoton microfabrication. Laser Photon Rev 2008;2:100–111.
[92] Palima D, Glückstad J. Gearing up for optical microrobotics: micromanipulation and actuation of synthetic microstructures by optical forces. Laser Photon Rev 2013;7:478–94.
[93] Glückstad J. Optical manipulation: sculpting the object. Nat Photon 2011;5:7–8.
[94] Montange RK, Bull MS, Shanblatt ER, Perkins TT. Optimizing bead size reduces errors in force measurements in optical traps. Opt Express 2013;21:39–48.
[95] Rodrigo PJ, Kelemen L, Palima D, Alonzo CA, Ormos P, Glückstad J. Optical microassembly platform for constructing reconfigurable microenvironments for biomedical studies. Opt Express 2009;17:6578–83.
[96] Phillips DB, Grieve JA, Olof SN, Kocher SJ, Bowman R, Padgett MJ, Miles MJ, Carberry DM. Surface imaging using holographic optical tweezers. Nanotechnology 2011;22:285503.
[97] Carberry D, Simpson S, Grieve J, Wang Y, Schäfer H, Steinhart M, Bowman R, Gibson G, Padgett M, Hanna S. Calibration of optically trapped nanotools. Nanotechnology 2010;21:175501.
[98] Neale SL, Macdonald MP, Dholakia K, Krauss TF. All-optical control of microfluidic components using form birefringence. Nat Mater 2005;4:530–3.
[99] Parkin SJ, Knöner G, Nieminen TA, Heckenberg NR, Rubinsztein-Dunlop H. Picoliter viscometry using optically rotated particles. Phys Rev E 2007;76 [doi: 10.1103/PhysRevE.76.041507].
[100] Wu TH, Chen Y, Park SY, Hong J, Teslaa T, Zhong JF, Di Carlo D, Teitell MA, Chiou PY. Pulsed laser triggered high speed microfluidic fluorescence activated cell sorter. Lab Chip 2012;12:1378–83.
[101] Simpson SH, Phillips DB, Carberry DM, Hanna S. Bespoke optical springs and passive force clamps from shaped dielectric particles. J Quant Spectrosc Radiat Transfer 2013;126:91–8.
[102] Hell SW, Wichmann J. Breaking the diffraction resolution limit by stimulated emission: stimulated-emission-depletion fluorescence microscopy. Opt Lett 1994;19:780–2.
[103] McLeod E, Arnold CB. Subwavelength direct-write nanopatterning using optically trapped microspheres. Nat Nanotechnol 2008;3:413–7.
[104] Nakayama Y, Pauzauskie PJ, Radenovic A, Onorato RM, Saykally RJ, Liphardt J, Yang P. Tunable nanowire nonlinear optical probe. Nature 2007;447:1098–101.
[105] Katsenelenbaum BZ. What is the direction of the poynting vector?. J Commun Technol Electron 1997;42:119–20.
[106] Novitsky AV, Novitsky DV. Negative propagation of vector Bessel beams. J Opt Soc Am A 2007;24:2844–9.
[107] Wong V, Ratner MA. Explicit computation of gradient and non-gradient contributions to optical forces in the discrete-dipole approximation. J Opt Soc Am B 2006;23:1801–14.
[108] Bouchal Z, Olivik M. Nondiffractive vector Bessel beams. J Mod Opt 1995;42:1555–66.
[109] Durnin J. Exact solutions for nondiffracting beams. I. The scalar theory. J Opt Soc Am A 1987;4:651.
[110] Bouchal Z, Wagner J, Chlup M. Self-reconstruction of a distorted nondiffracting beam. Opt Comm 1998;151:207–11.
[111] Turunen J, Friberg AT. Self-imaging and propagation-invariance in electromagnetic fields. Pure Appl Opt 1993;2:51–60.
[112] Salem MA, Bağcı H. Energy flow characteristics of vector X-Waves. Opt Express 2011;19:8526–32.
[113] Siviloglou GA, Christodoulides DN. Accelerating finite energy Airy beams. Opt Lett 2007;32:979–81.
[114] Berry M, Balazs N. Nonspreading wave packets. Am J Phys 1979;47:264–7.
[115] Novitsky AV, Novitsky DV. Nonparaxial Airy beams: role of evanescent waves. Opt Lett 2009;34:3430–2.
[116] Vaveliuk P, Martinez-Matos O. Negative propagation effect in nonparaxial Airy beams. Opt Express 2012;20:26913–21.
[117] Ashkin A, Gordon JP. Cooling and trapping of atoms by resonance radiation pressure. Opt Lett 1979;4:161–3.
[118] Hansch TW, Schawlow AL. Cooling of gases by laser radiation. Opt Comm 1975;13:68–9.
[119] Kasevich M, Chu S. Laser cooling below a Photon Recoil with three-level atoms. Phys Rev Lett 1992;69:1741–4.
[120] Jacquinot P, Liberman S, Picqué J-L, Pinard J. High resolution spectroscopic application of atomic beam deflection by resonant light. Opt Comm 1973;8:163–5.
[121] Ashkin A, Dziedzic JM. Optical trapping and manipulation of viruses and bacteria. Science 1987;235:1517–20.
[122] Ashkin A, Dziedzic JM, Yamane T. Optical trapping and manipulation of single cells using infrared laser beams. Nature 1987;330:769–71.
[123] Liang H, Vu KT, Krishnan P, Trang TC, Shin D, Kimel S, Berns MW. Wavelength dependence of cell cloning efficiency after optical trapping. Biophys J 1996;70:1529–33.
[124] Liang H, Wright WH, Cheng S, He W, Berns MW. Micromanipulation of chromosomes in PtK2 cells using laser microsurgery (optical scalpel) in combination with laser-induced optical force (optical tweezers). Exp Cell Res 1993;204:110–20.
[125] Ashkin A, Dziedzic JM. Optical levitation by radiation pressure. Appl Phys Lett 1971;19:283–5.
[126] Ashkin A, Dziedzic JM. Stability of optical levitation by radiation pressure. Appl Phys Lett 1974;24:586–8.
[127] Marston PL. Negative axial radiation forces on solid spheres and shells in a Bessel beam (L). J Acoust Soc Am 2007;122:3162–5.
[128] Marston PL. Scattering of a Bessel beam by a sphere. J Acoust Soc Am 2007;121:753–8.
[129] Garcia-Etxarri A, Gomez-Medina R, Froufe-Perez LS, Lopez C, Chantada L, Scheffold F, Aizpurua J, Nieto-Vesperinas M,

Saenz JJ. Strong magnetic response of submicron silicon particles in the infrared. Opt Express 2011;19:4815–26.
[130] Nieto-Vesperinas M, Gomez-Medina R, Saenz JJ. Angle-suppressed scattering and optical forces on submicrometer dielectric particles. J Opt Soc Am A 2011;28:54–60.
[131] Čižmár T, Kollárová V, Bouchal Z, Zemánek P. Sub-micron particle organization by self-imaging of non-diffracting beams. N J Phys 2006;8:43.
[132] Kerker M, Wang DS, Giles CL. Electromagnetic scattering by magnetic spheres. J Opt Soc Am 1983;73:765–7.
[133] García-Cámara B, de la Osa RA, Saiz JM, González F, Moreno F. Directionality in scattering by nanoparticles: Kerker's null-scattering conditions revisited. Opt Lett 2011;36:728–30.
[134] García-Cámara B, González F, Moreno E, Saiz JA. Exception for the zero-forward-scattering theory. J Opt Soc Am A 208;25:2875–78.
[135] Geffrin JM, García-Cámara B, Gómez-Medina R, Albella P, Froufe-Pérez LS, Eyraud C, Litman A, Vaillon R, González F, Nieto-Vesperinas M, Sáenz JJ, Moreno F. Magnetic and electric coherence in forward- and back-scattered electromagnetic waves by a single dielectric subwavelength sphere. Nat Commun 2012;3:1171.
[136] Luk'yanchuk B, Zheludev NI, Maier SA, Halas NJ, Nordlander P, Giessen H, Chong CT. The Fano resonance in plasmonic nanostructures and metamaterials. Nat Mater 2010;9:707–15.
[137] Gómez-Medina R, García-Cámara B, Suárez-Lacalle I, González F, Moreno F, Nieto-Vesperinas M, Sáenz JJ. Electric and magnetic dipolar response of germanium nanospheres: interference effects, scattering anisotropy, and optical forces. J Nanophoton 2011;5:053512.
[138] Sáenz JJ. Optical forces: laser tractor beams. Nat Photon 2011;5:514–5.
[139] Khonina S, Kotlyar V, Skidanov R, Soifer V, Jefimovs K, Simonen J, Turunen J. Rotation of microparticles with Bessel beams generated by diffractive elements. J Mod Opt 2004;51:2167–84.
[140] Dogariu A, Sukhov S, Sáenz JJ. Optically induced 'negative forces'. Nat Photon 2013;7:24–7.